

$\theta \approx \theta_a$ . In the other extreme, when  $\theta = 0.4$  arcsec, the magnetic field from the magnetar would be negligible, but the inferred field strength can be easily explained as arising from compression of the ambient field by the bow shock. The mean expansion speed of the nebula is  $3.5 \times 10^{10} d_5 \theta_{10}^{-1} \text{ cm s}^{-1}$  where  $t_{10}$  is the age of the nebula in units of 10 days. Thus in the limit of  $\theta = 0.4$  arcsec the nebula would have expanded relativistically. This is possible if previous outbursts have swept up the ambient gas. In this limit,  $U_{\text{min}}$  is comparable with the isotropic burst energy of  $3 \times 10^{42} d_5^2 \text{ erg}$ , as estimated from the fluence of the 27 August burst ( $\sim 10^{-3} \text{ erg cm}^{-2}$ ; M. Feroci, personal communication). In either case, it is clear that nebular expansion accounts for the rapidly decaying radio emission. Thus the above energy estimates (derived from observations 7–10 days after the burst) need to be revised upwards to obtain the initial release of energy.

In the future, the availability of broad-band observations and/or direct measurement of the size of the nebula should enable us to estimate directly the energy of the burst in particles (without the uncertainties of beaming that bedevil estimates from  $\gamma$ -ray data). Equally important are accurate measurements of the average particle luminosity, as particle-aided spindown can substantially modify estimates for the magnetic field and the characteristic age of a neutron star<sup>21</sup>. These estimates, to our knowledge, are unobtainable in any other fashion. In those cases where the SGR is immersed in a high-pressure region (for example, SGR1806–20), we are able to trace the entire history of energy loss from the magnetar. The sub-arcsecond localization presented here should greatly help the identification of possible stellar counterparts of this SGR (as was done for SGR1806–20; refs 22, 23). □

Received 28 October; accepted 21 December 1998.

1. Kulkarni, S. R. & Frail, D. A. Identification of a supernova-remnant coincident with the soft  $\gamma$ -ray repeater SGR1806–20. *Nature* **365**, 33–35 (1993).
2. Thompson, C. & Duncan, R. C. The soft gamma repeaters as very strongly magnetized neutron stars—I. Radiative mechanism for outbursts. *Mon. Not. R. Astron. Soc.* **275**, 255–300 (1995).
3. Thompson, C. & Duncan, R. C. The soft gamma repeaters as very strongly magnetized neutron stars. II. Quiescent neutrino, X-ray, and Alven wave emission. *Astrophys. J.* **473**, 322–342 (1996).
4. Mazets, E. P., Golenetskii, S. V., Il'inskiii, V. N., Aptekar', R. L. & Gur'yan, Yu. A. Observations of a flaring X-ray pulsar in Dorado. *Nature* **282**, 587–589 (1979).
5. Kouveliotou, C. *et al.* An X-ray pulsar with a super-strong magnetic field in the soft  $\gamma$ -ray repeater SGR1806–20. *Nature* **393**, 235–237 (1998).
6. Hurley, K. *et al.* A giant periodic flare from the soft  $\gamma$ -ray repeater SGR1900+14. *Nature* **397**, 41–43 (1999).
7. Cline, T. L., Mazets, E. P. & Golenetskii, S. V. *IAU Circ. No.* 7002 (1998).
8. Mazets, E. P., Golenetskii, S. V. & Gur'yan, Yu. A. Soft gamma-ray bursts from the source B1900+14. *Sov. Astron. Lett.* **5**, 343–344 (1979).
9. Kouveliotou, C. *et al.* Recurrent burst activity from the soft  $\gamma$ -ray repeater SGR1900+14. *Nature* **362**, 728–730 (1993).
10. Vasishth, G., Kulkarni, S. R., Frail, D. A. & Griener, G. Supernova candidates for the soft  $\gamma$ -ray repeater 1900+14. *Astrophys. J.* **431**, L35–L38 (1994).
11. Kouveliotou, C. *et al.* The rarity of soft  $\gamma$ -ray repeaters deduced from reactivation of SGR1806–20. *Nature* **368**, 125–127 (1994).
12. Hurley, K. *et al.* Network synthesis localization of two soft gamma repeaters. *Astrophys. J.* **431**, L31–L34 (1994).
13. Hurley, K. *et al.* A possible X-ray counterpart to SGR 1900+14. *Astrophys. J.* **463**, L13–L16 (1996).
14. Windhorst, R. A., Fomalont, E. B., Partridge, R. B. & Lowenthal, J. D. *Astrophys. J.* **405**, 498–517 (1993).
15. Murakami, T. *et al.* X-ray identification of the soft  $\gamma$ -ray repeater 1806–20. *Nature* **368**, 127–129 (1994).
16. Kulkarni, S. R., Frail, D. A., Kassim, N. E., Murakami, T. & Vasishth, G. The radio nebula of the soft  $\gamma$ -ray repeater 1806–20. *Nature* **368**, 129–131 (1994).
17. Vasishth, G., Frail, D. A. & Kulkarni, S. R. Radio monitoring and high-resolution imaging of the soft gamma-ray repeater 1806–20. *Astrophys. J.* **440**, L65–L68 (1995).
18. Frail, D. A., Vasishth, G. & Kulkarni, S. R. The changing structure of the radio nebula around the soft gamma-ray repeater SGR 1806–20. *Astrophys. J.* **480**, L129–L132 (1997).
19. Pacholczyk, A. G. *Radio Astrophysics* Ch. 7 (Freeman, San Francisco, 1970).
20. Scott, M. A. & Readhead, A. C. S. The low frequency structure of powerful radio sources and limits to departures from equipartition. *Mon. Not. R. Astron. Soc.* **180**, 539–550 (1977).
21. Thompson, C. & Blaes, O. Magnetohydrodynamics in the extreme relativistic limit. *Phys. Rev. D* **57**, 3219–3234 (1998).
22. Kulkarni, S. R. *et al.* Optical and infrared observations of SGR 1806–20. *Astrophys. J.* **440**, L61–L64 (1995).
23. van Kerkwijk, M. H., Kulkarni, S. R., Matthews, K. & Neugebauer, G. A luminous companion to SGR 1806–20. *Astrophys. J.* **44**, L33–L35 (1995).

**Acknowledgements.** The National Radio Astronomy Observatory is a facility of the NSF operated under cooperative agreement by Associated Universities, Inc. D.A.F. thanks C. Thompson and M. Goss for discussions. We thank B. Clark and M. Goss for their long-term support in the search for SGR1900+14. S.R.K. is supported by the NSF and NASA.

Correspondence and requests for materials should be addressed to D.A.F. (e-mail: dfrail@nrao.edu).

## Rotation rates of Kuiper-belt objects from their light curves

W. Romanishin\* & S. C. Tegler†

\* Department of Physics & Astronomy, University of Oklahoma, Norman, Oklahoma 73019, USA

† Department of Physics & Astronomy, Northern Arizona University, Flagstaff, Arizona 86011, USA

Very little is known about the physical properties of Kuiper-belt objects<sup>1</sup>, due to their relatively small size and large distance from the Earth. For example, a Kuiper-belt object with a diameter of 300 km at a typical distance of  $\sim 30$  AU would subtend an angle of only 0.014 arcsec. It is therefore possible to investigate their surface markings, shapes and rotational properties only through variations in the light that they reflect (their light curves). Here we report a survey of optical light curves from Kuiper-belt objects. Variations are observed only for the faintest objects in the survey. We can rule out eclipsing binary objects and variations in the surface markings as the origin of these light curves, suggesting that the observed variations are due to the rotation of irregularly shaped objects. Irregular shapes may be limited to the smallest Kuiper-belt objects because the material strength in their inner regions is sufficient to maintain the shape against the weight of the overlying material. If, however, all of the objects in our survey are of essentially the same size, then the intrinsically faintest ones may be composed of a stronger and darker material than the brighter ones.

Because Kuiper-belt objects (KBOs) are too faint for thermal infrared observations with a high signal-to-noise ratio, visible and near-infrared photometry seem to be the only way to learn anything about their diameters, shapes and surface markings. The diameter,  $D$  (in kilometres), of a KBO can be obtained from the definition of albedo,  $p$ :

$$p\Phi D^2 = 9 \times 10^{16} r^2 \Delta^2 10^{0.4(m_{\odot} - V)} \quad (1)$$

where  $\Phi$  is the phase function<sup>2</sup>,  $r$  is the heliocentric distance (AU),  $\Delta$  is the geocentric distance (AU),  $m_{\odot}$  is the apparent V-band solar magnitude (–26.74), and  $V$  is the apparent V-band magnitude of the KBO. The diameters that we derive below assume an albedo similar to that of the progeny of the KBOs—the nuclei of short-period comets. Such nuclei have  $p = 0.04$ , implying a surface as black as charcoal.

The shape or surface markings of a KBO can be derived from periodic variations in its brightness. In the case of a spherical KBO with light and dark surface markings (for example, with one hemisphere darker on average than the other), each rotation of the KBO results in one minimum and one maximum in the light curve. If the KBO has a uniform surface albedo, but an elongated shape, rotation of the object results in a periodic variation of the projected cross-sectional area. Each rotation of the elongated object results in two minima and two maxima in the light curve. The amplitude of the light curve,  $\Delta m$ , is related to the major axis,  $a$ , and the intermediate axis,  $b$ , of a triaxial object by the equation:

$$\Delta m = 2.5 \log \frac{a}{b} \quad (2)$$

where we have assumed that the axis of rotation is perpendicular to the line of sight (an 'equator-on' aspect) and lies along the short axis,  $c$ , of the body. The determination of the orientation of the rotation axis of a KBO from photometry would require data from about one-quarter of a KBO revolution about the Sun, about 40 years for a KBO at 30 AU. Such a determination is beyond the scope of this survey and therefore requires our simplifying assumption.

Our KBO survey uses Harris V (550 nm) and R (650 nm) 5 × 5 inch glass filters in front of a 1,200 × 800 pixel charge-coupled-device (CCD) camera at the *f*/9 Cassegrain focus of the Steward Observatory 2.3-m telescope on Kitt Peak, Arizona. The results presented here and in our KBO colour survey<sup>3–6</sup> use the same data sets; the details of our observing and data-reduction procedures are contained in these earlier reports. We mention here that our aperture correction technique not only minimizes the sky noise in our measurements, but also minimizes errors due to contamination by faint galaxies and stars. An estimate of the effects due to contamination by faint background objects can be found by looking at the number–magnitude counts<sup>7,8</sup> of faint stars and galaxies made to *R*-band magnitude *R* = 25 at relatively high Galactic latitudes, where many of the known KBOs are found. Extrapolating the number–magnitude relation to *R* = 26 mag, we find that the number of galaxies per degree<sup>2</sup> is larger than the number of stars per degree<sup>2</sup>, and that there are about 2.5 × 10<sup>5</sup> galaxies per degree<sup>2</sup> between *R* = 23 mag and *R* = 26 mag; this corresponds to ~0.02 galaxy per arcsec<sup>2</sup>. By using an aperture three pixels in radius for our KBO measurements, we greatly decrease our chances of including an ‘unseen’ (fainter than *R* = 23 mag) faint galaxy. The chance of finding a galaxy between *R* = 23 mag and *R* = 26 mag in our small aperture are 1 in 20.

Our V-band photometry is summarized in columns 2 and 3 of Table 1. An important aspect of our programme is that our photometry is consistent over intervals of hours, days and years. We find that 25 V-band magnitude measurements of the KBO 1996 TL66 taken over a time interval of seven days yield a standard deviation about the mean of 0.03 mag (Table 1). We obtain a similar consistency for 1996 TO66. Individual V-band magnitudes of the KBO 1993 SC agree at the 0.06-mag level over intervals of hours and days<sup>6</sup>. Once we correct for differences in distances and phase angle using a slope parameter of 0.15, we find that our V-band magnitudes for 1993 SC and 1994 TB are consistent at the 0.07-mag level over an interval of nearly a year and two years, respectively. Such repeatability in our photometry supports our hypothesis that contamination by faint stars and galaxies is not an important source of error in our KBO measurements.

We now consider how our photometry compares with that of other investigators. As there is little agreement between investigators regarding the *B* – *V* and *V* – *R* colours of KBOs<sup>4</sup>, we will confine our comparison to V-band magnitudes. First, we find that Jewitt and Luu<sup>9</sup> observed the brightest KBOs (1996 TS66, 1996 TP66, 1996 TO66 and 1996 TL66) on 23 and 24 September 1997, about a week

before our measurements. For three of the four KBOs, our V-band magnitudes (Table 1) and their magnitudes differ by ≤0.05 mag, a remarkably good agreement. For an unknown reason, our colours and their colours for these same objects exhibit far less agreement. Second, we consider studies of the Centaur, 5145 Pholus. Buie and Bus<sup>10</sup> and Davies *et al.*<sup>11</sup> obtain absolute magnitudes (brightness at unit heliocentric and geocentric distance and 0° phase angle), *H*<sub>V</sub>, of 7.645 ± 0.011 and 7.63 ± 0.02, respectively, for 5145 Pholus. We obtain *H*<sub>V</sub> = 7.63 ± 0.03 mag for 5145 Pholus, again very good agreement. Last, Davies *et al.* find good agreement between our V-band magnitudes and *V* – *R* colours and their V-band magnitudes and *V* – *R* colours for the Centaurs in their study.

There are 12 objects in Table 1 that have sufficient temporal coverage for use to measure, or set limits on, the amplitudes of light curves (see column 6 of Table 1). Of the KBOs, only 1995 QY9, 1994 VK8 and 1994 TB (November 1995 and October 1997) exhibit detectable brightness variations (Fig. 1). We have analysed the light curves in Fig. 1 using the techniques of phase dispersion minimization<sup>12</sup> as well as a phasing of the data with every possible period between 1 and 10 hours. We find that 1995 QY9 has a best period of ~3.5 hours, and a viable range of periods that extends between 3.3 and 3.7 hours. For 1994 VK8, we find possible light-curve periods of 3.9, 4.3, 4.7 and 5.2 hours. In the case of 1994 TB, we find that possible periods of 3.0 and 3.5 hours fit both the 1995 and 1997 data.

These periods are so short that they eliminate the rotation of essentially spherical objects with light and dark surface markings (for example, one hemisphere darker on average than the other) as the mechanism responsible for the light curves. Applying Newton’s second law of motion and the law of gravitation allows us to calculate the period, *P*<sub>crit</sub>, at which a KBO rotates so fast that it will throw material off its equator and hence be unlikely to retain a regolith or even to form in the first place by accretion:

$$P_{\text{crit}} = \left( \frac{3\pi}{G\rho} \right)^{\frac{1}{2}} \quad (3)$$

where  $\rho$  is the density. If we assume  $\rho = 1 \text{ g cm}^{-3}$ , we obtain *P*<sub>crit</sub> = 3.3 hours. Our measured periods are slightly below, at, or slightly above, the critical period, making it unlikely that light and dark surface markings are responsible for the light curves.

The short measured periods make it unlikely that eclipsing binary KBOs are responsible for the light curves. The shortest period allowed for a binary KBO system corresponds to a separation

**Table 1 Properties of KBOs**

Object	<i>V</i> (mag)	$\sigma$ (mag)	<i>n</i>	<i>H</i> <sub>V</sub> (mag)	$\Delta m$ (mag)	<i>D</i> (km)	<i>a/b</i>	UT Date
1997 CU26	18.56	0.02	2	6.75		300		8 Oct. 1997
1997 CS29	22.11	0.11	12	5.52	≤0.22	530	≤1.22	6, 9, 10 Oct. 1997
1996 TS66	22.47	0.08	7	6.50	≤0.16	340	≤1.16	5 Oct. 1997
1996 TQ66	23.12	0.11	10	7.69	≤0.22	200	≤1.22	4 Oct. 1997
1996 TP66	21.64	0.06	16	7.39	≤0.12	220	≤1.12	3–5 Oct. 1997
1996 TO66	21.38	0.05	13	4.75	≤0.10	760	≤1.10	3, 4, 6 Oct. 1997
1996 TL66	20.91	0.03	25	5.40	≤0.06	560	≤1.06	2, 9 Oct. 1997
1996 RQ20	22.94	0.07	7	6.99		270		10 Oct. 1997
1995 QY9	22.88		11	8.07	0.60	160	1.74	10 Oct. 1997
1995 HM5	23.4	0.1	3	8.30		150		8 Apr. 1997
1995 GO	20.12		15	9.19	0.34	100	1.37	14 Apr. 1996
1995 DW2	22.24	0.02	7	9.53	≤0.04	84	≤1.04	7 Apr. 1997
1994 VK8	24.05		15	7.53	0.42	210	1.47	24, 26 Jan. 1998
1994 TB	22.91		12	8.04	0.26	166	1.27	7 Oct. 1997
	23.20		12	8.11	0.34	161	1.37	24–27 Nov. 1995
1994 JR1	22.9	0.1	5	7.35		230		7, 8 Apr. 1997
1993 SC	22.74	0.02	4	7.23	≤0.04	240	≤1.04	24–27 Nov. 1995
	22.67	0.06	8	7.30	≤0.12	230	≤1.12	8 Oct. 1996
Nessus	20.84	0.04	2	9.52		80		14 Apr. 1996
Pholus	18.46	0.05	3	7.63	0.15 <sup>9</sup>	200		27 Nov. 1995

Meaning of symbols is as follows. *V*, Average V-band magnitude;  $\sigma$ , standard deviation about the average; *n*, number of images averaged; *H*<sub>V</sub>, absolute magnitude;  $\Delta m$ , light-curve amplitude (objects without entries do not have sufficient temporal coverage to measure or set an upper limit on an amplitude); *D*, diameter, assuming a cometary albedo of 0.04; *a/b*, major-to-intermediate axial ratio, assuming that the axis of rotation is perpendicular to our line of sight.

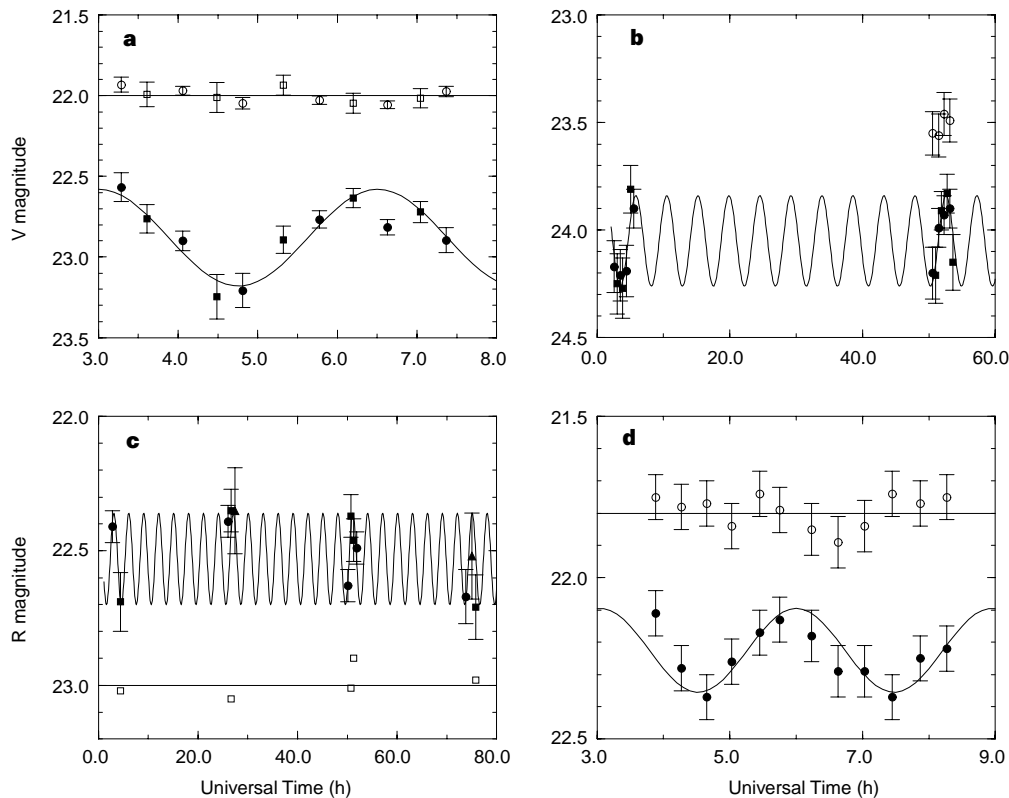


**Figure 1** Light curves for Kuiper-belt objects (filled symbols) and faint field stars (open symbols). Measurements through the V and R filters are plotted as squares and circles, respectively. Conversions between V-band and R-band magnitudes are accomplished with the  $V - R$  colours of the objects. All error bars are  $\pm 1\sigma$  and are a measure of the sky noise. All sine curves represent possible periods and amplitudes obtained from our phase dispersion minimization and phasing techniques. **a**, V magnitudes for 1995 QY9 and a faint field star. The data from the star have been moved upwards on the figure for clarity; the actual average V magnitude and standard deviation of the star are 22.46 and 0.04, respectively.

The sine curve has a period of 3.5 h and an amplitude of 0.60 mag. **b**, V magnitudes for the KBO 1994 VK8 and a faint field star. The sine curve has a period of 4.7 h and an amplitude of 0.42 mag. **c**, R magnitudes obtained between 24 and 27 November 1995 for the KBO 1994 TB. The sine curve has a period of 3.0 h and an amplitude of 0.34 mag. **d**, R magnitudes obtained on 7 October 1997 for the KBO 1994 TB and a faint star. The data from the faint field star have been moved upwards for clarity; the actual R magnitude of the star is 22.19. The sine curve has a period of 3.0 h and an amplitude of 0.26 mag.

distance equal to the sum of the radii of the KBOs. If we assume similar sizes and densities for the two KBOs, then application of Newton's second law and the law of gravitation yields:

$$P_{\text{binary}} = \left( \frac{12\pi}{G\rho} \right)^{\frac{1}{2}} \quad (4)$$

If we assume a density of  $1 \text{ g cm}^{-3}$ , we obtain a minimum period of revolution for the binary of 6.6 hours. Because a complete cycle of the binary corresponds to two minima and two maxima in the light curve, we must double our KBO light-curve periods for comparison with the 6.6-hour minimum period for the binary. Once again, our measured periods are slightly below, at, or slightly above, the binary limit, making it unlikely that eclipsing binaries are responsible for the light curves.

Now that we have eliminated surface markings and binaries as mechanisms, it seems that our light curves are due to the rotation of irregularly shaped bodies. On doubling the light-curve periods, we find rotation periods of  $\sim 7.0$  hours for 1995 QY9, possible periods of 7.8, 8.6, 9.4 and 10.4 hours for 1994 VK8, and 6.0 and 7.0 hours for 1994 TB. As a comparison, a histogram of rotation periods of asteroids with  $125 \leq D \leq 200 \text{ km}$  has a peak at 12 hours (ref. 13).

We have also analysed the amplitudes of the light curves. A plot of the light-curve amplitude, and the  $2\sigma$  upper limit for an amplitude, against absolute visual magnitude ( $H_V$ ) for the 12 KBOs is shown in Fig. 2. A clear pattern can be seen in this figure: the intrinsically

brightest objects show no evidence of any significant brightness variation, whereas the intrinsically faintest objects do show such a variation.

The trend in Fig. 2 has two possible explanations. First, the KBOs in our sample could all have the same albedo: the difference in intrinsic brightness among the objects would then be due to differences in size. In the central region of a small KBO, the material strength exceeds the weight exerted by the overlying material. A small KBO can therefore be strong enough to retain any irregularity in its shape. In the central region of a very large KBO, on the other hand, the overlying weight of material exceeds the material strength, and crushes any irregularities in shape. Large KBOs must therefore take on a spherical shape. If we consider the diameter at which the transition between irregular and spherical KBOs takes place,  $D_t$ , we can estimate the strength of KBO material. If we assume a constant density throughout a KBO, then application of the equation of hydrostatic equilibrium at a radial distance of  $0.8R$  from the KBO centre yields an expression for the material strength:

$$S = 1.29 \times 10^{-8} D_t^2 \rho^2 \quad (5)$$

where  $S$  is in  $\text{dyn cm}^{-2}$  and  $D_t$  is in cm. We chose a radius of  $0.8R$  because half the mass of the KBO is inside such a radius, and the mechanical failure of ice at such a radius will probably manifest itself in terms of topographic relaxation in shape. An examination of column 7 in Table 1 suggests that the transition diameter occurs

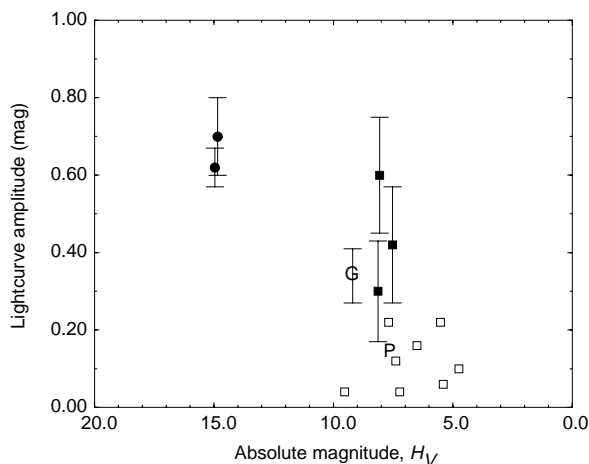


**Figure 2** A plot of the light-curve amplitude versus the absolute magnitude for the 12 objects in our survey with good temporal coverage. The open squares and filled squares represent upper limits and  $\Delta m$  detections, respectively. The filled circles represent  $\Delta m$  detections for the bare nuclei of short-period comets<sup>19,20</sup>. The symbols P and G represent the Centaurs 5145 Pholus<sup>10</sup> and 1995 GO<sup>311,21</sup>. A pattern is clearly seen; intrinsically faint KBOs exhibit light curves.

around 250 km, assuming an albedo of 0.04. If we assume a density of  $1 \text{ g cm}^{-3}$ , we obtain a material strength of  $8 \times 10^6 \text{ dyn cm}^{-2}$ , a value smaller than that of a bulk ice in a laboratory<sup>14</sup>,  $2 \times 10^7 \text{ dyn cm}^{-2}$ . Larger objects are known to be weaker than smaller objects of the same material. Models of size-dependent strength<sup>15</sup> imply that strength should scale as  $R^{-3/(m+3)}$  where  $m = 8.1$  for ice. Thus the models suggest that the strength of a KBO with  $R = 100 \text{ km}$  should be  $(10^7)^{-0.27} (= 0.01)$  times the laboratory strength of ice, that is,  $\sim 2 \times 10^5 \text{ dyn cm}^{-2}$ .

The second possibility that can explain the trend in Fig. 2 is that the KBOs in our sample are all about the same size. The difference in intrinsic brightness would then be due to differences in albedo, the intrinsically faint objects being composed of a darker material than the brighter objects. If the dark material has a greater material strength than the lighter material, the dark objects could support more overlying material and hence retain their irregular shapes to greater diameters than could the light-coloured KBOs (E. Asphaug, personal communication).

What mechanism is responsible for the production of irregularly shaped objects? One possibility is that the objects in our survey retained their original shapes from the time they stopped growing. An alternative possibility is that the irregular shapes are shards from collisions. Calculations<sup>16–18</sup> have shown that objects with diameter  $>100 \text{ km}$  cannot be shattered by collisions in the present-day Kuiper belt; this is because collisions between such large targets and impactors that are large enough to disrupt these targets are too infrequent. If the KBOs have albedos similar to those of short-period comets, then their irregular shapes are the result of primordial formation processes. □

Received 13 October 1998; accepted 4 January 1999.

- Levison, H. F. & Weisman, P. R. in *The Encyclopedia of the Solar System* (eds Weisman, P. R., McFadden, L. A. & Johnson, T.) 557–582 (Academic, New York, 1999).
- Bowell, E. B. *et al.* in *Asteroids II* (eds Binzel, R., Gehrels, T. & Matthews, M.) 524–556 (Univ. Arizona Press, Tucson, 1989).
- Romanishin, W., Tegler, S. C., Levine, J. & Butler, N. BVR photometry of centaur objects 1995 GO, 1993 HA2, and 5145 Pholus. *Astron. J.* **113**, 1893–1898 (1997).
- Tegler, S. C. & Romanishin, W. Two distinct populations of Kuiper belt objects. *Nature* **392**, 49–51 (1998).
- Tegler, S. C. & Romanishin, W. The extraordinary colors of 1994 TB and 1993 SC. *Icarus* **126**, 212–217 (1997).
- Tegler, S. C. *et al.* Photometry of the trans-neptunian object 1993 SC. *Astron. J.* **114**, 1230–1233 (1997).
- Hintzen, P., Romanishin, W. & Valdes, F. Galaxies clustering around QSOs with  $z = 0.9–1.5$  and the origin of blue field galaxies. *Astrophys. J.* **366**, 7–15 (1991).
- Trentham, N. The luminosity function of dwarf galaxies in four spiral-rich clusters. *Mon. Not. R. Astron. Soc.* **286**, 133–157 (1997).
- Jewitt, D. & Luu, J. Optical-infrared spectral diversity in the Kuiper belt. *Astron. J.* **115**, 1667–1670 (1998).

- Buie, M. W. & Bus, S. J. Physical observations of 5145 Pholus. *Icarus* **100**, 288–294 (1992).
- Davies, J. K., McBride, N., Ellison, S. L., Green, S. F. & Ballantyne, D. R. Visible and infrared photometry of six centaurs. *Icarus* **134**, 213–227 (1998).
- Schleicher, D. G. *et al.* Periodic variations in the activity of Comet P/Halley during the 1985/1986 apparition. *Astron. J.* **100**, 896–912 (1990).
- Binzel, R., Farinella, P., Zappala, V. & Cellino, A. in *Asteroids II* (eds Binzel, R., Gehrels, T. & Matthews, M.) 416–441 (Univ. Arizona Press, Tucson, 1989).
- Hobbs, P. V. *Ice Physics* (Clarendon, Oxford, 1974).
- Asphaug, E. *et al.* Mechanical and geological effects of impact cratering on Ida. *Icarus* **120**, 158–184 (1996).
- Stern, S. A. Collisional time scales in the Kuiper disk and their implications. *Astron. J.* **110**, 856–868 (1995).
- Farinella, P. & Davis, D. R. Short-period comets: primordial bodies or collisional fragments? *Science* **273**, 938–941 (1996).
- Stern, S. A. Signatures of collisions in the Kuiper disk. *Astron. Astrophys.* **310**, 999–1010 (1996).
- Jewitt, D. C. & Luu, J. X. A CCD portrait of comet P/Tempel 2. *Astron. J.* **97**, 1766–1790 (1989).
- Luu, J. X. & Jewitt, D. C. The nucleus of comet P/Encke. *Icarus* **86**, 69–81 (1990).
- Brown, W. R. & Luu, J. X. CCD photometry of the Centaur 1995 GO. *Icarus* **126**, 218–224 (1997).

**Acknowledgements.** We thank D. Schleicher for application of his phase dispersion minimization and phasing software to the KBO lightcurves, and E. Asphaug and J. Davies for comments on the manuscript. We also thank the Steward Observatory Telescope Allocation Committee for telescope time. This work was supported by the NASA Origins of Solar Systems and Planetary Astronomy programs.

Correspondence and requests for materials should be addressed to W.R. (e-mail: wjr@mail.nhn.ou.edu).

## Quantum-well states in copper thin films

R. K. Kawakami\*, E. Rotenberg†, Hyuk J. Choi\*, Ernesto J. Escorcia-Aparicio\*, M. O. Bowen\*, J. H. Wolfe\*, E. Arenholz\*, Z. D. Zhang\*‡, N. V. Smith† & Z. Q. Qiu\*

\* Department of Physics, University of California at Berkeley, Berkeley, California 94720, USA

† Advanced Light Source, Lawrence Berkeley National Laboratory, Berkeley, California 94720, USA

A standard exercise in elementary quantum mechanics is to describe the properties of an electron confined in a potential well. The solutions of Schrödinger's equation are electron standing waves—or 'quantum-well' states—characterized by the quantum number  $n$ , the number of half-wavelengths that span the well. Quantum-well states can be experimentally realized in a thin film, which confines the motion of the electrons in the direction normal to the film: for layered semiconductor quantum wells, the aforementioned quantization condition provides (with the inclusion of boundary phases) a good description of the quantum-well states. The presence of such states in layered metallic nanostructures is believed to underlie many intriguing phenomena, such as the oscillatory magnetic coupling of two ferromagnetic layers across a non-magnetic layer<sup>1,2</sup> and giant magnetoresistance<sup>3</sup>. But our understanding of the properties of the quantum-well states in metallic structures is still limited. Here we report photoemission experiments that reveal the spatial variation of the quantum-well wavefunction within a thin copper film. Our results confirm an earlier proposal<sup>4</sup> that the amplitude of electron waves confined in a metallic thin film is modulated by an envelope function (of longer wavelength), which plays a key role in determining the energetics of the quantum-well states.

The standard quantization condition on an electron of wavevector  $k$  within a potential well of width  $d$  is:

$$2kd + \phi = 2\pi n \quad (1)$$

This equation expresses the requirement that, as the electron 'bounces' back and forth within the well, the length of a round trip must (apart from end corrections embodied in the phase  $\phi$ ) equal an integral number of wavelengths. For fixed  $n$ , an increase of  $d$  results in a decrease of  $k$ . Because the conduction electron's

‡ Permanent address: International Center for Materials Physics, Institute of Metal Research, Academia Sinica, Shenyang 110015, People's Republic of China.